Electric field versus surface alignment in confined films of a diblock copolymer melt

Electric field versus surface alignment in confined films of a diblock copolymer melt

Andriy V. Kyrylyuk[a)]
Theoretical and Polymer Physics Group, Department of Applied Physics, Eindhoven University of Technology, P.O. Box 513, 5600 MB Eindhoven, The Netherlands and Dutch Polymer Institute, P.O. Box 902, 5600 AX Eindhoven, The Netherlands

Johannes G. E. M. (Hans) Fraaije
Soft Matter Chemistry Group, Leiden Institute of Chemistry, Leiden University, P.O. Box 9502, 2300 RA Leiden, The Netherlands

(Received 29 June 2006; accepted 15 September 2006; published online 30 October 2006; publisher error corrected 1 November 2006)

The dynamics of alignment of microstructure in confined films of diblock copolymer melts in the presence of an external electric field was studied numerically. We consider in detail a symmetric diblock copolymer melt, exhibiting a lamellar morphology. The method used is a dynamic mean-field density functional method, derived from the generalized time-dependent Ginzburg-Landau theory. The time evolution of concentration variables and therefore the alignment kinetics of the morphologies are described by a set of stochastic equations of a diffusion form with Gaussian noise. We investigated the effect of an electric field on block copolymers under the assumption that the long-range dipolar interaction induced by the fluctuations of composition pattern is a dominant mechanism of electric-field-induced domain alignment. The interactions with bounding electrode surfaces were taken into account as short-range interactions resulting in an additional term in the free energy of the sample. This term contributes only in the vicinity of the surfaces. The surfaces and the electric field compete with each other and align the microstructure in perpendicular directions. Depending on the ratio between electric field and interfacial interactions, parallel or perpendicular lamellar orientations were observed. The time scale of the electric-field-induced alignment is much larger than the time scale of the surface-induced alignment and microphase separation. © *2006 American Institute of Physics*. [DOI: 10.1063/1.2360947]

I. INTRODUCTION

It is well known that many self-assembled systems organize themselves in ordered morphologies, exhibiting long-range orientation of mesoscopic morphologies such as lamellar, hexagonally packed cylindrical, body-centered cubic spherical, gyroid bicontinuous, etc. Examples are block copolymer systems,[1,2] which are formed from several chemically different polymer blocks covalently attached at their ends. The incompatibility of monomers gives rise to various order-disorder transitions (ODTs). Block copolymer liquids have a strong tendency to segregate into ordered patterns of microdomains. The size of ordered microdomains is determined by the polymer chain lengths of different blocks and ranges between tens of nanometers. The morphology of a block copolymer nanostructure depends mainly on the temperature and the volume fraction of the polymer blocks.[1,2]

Block copolymer materials are used in numerous industrial applications. The production of a new material with certain desired macroscale properties requires modification of the normal mesoscale phase behavior by external factors. These factors can be surfaces,[3] confinements,[4,5] and diverse external fields such as magnetic fields,[6,7] hydrodynamical fields,[8,9] electric fields,[10–40] and mechanical deformations.[41]

Recently, considerable attention has been paid to the effects of electric fields on phase behavior of various polymeric systems, such as blends,[42–45] solutions,[46–52] and melts[10–40] in the vicinity of phase transitions. Alignment of block copolymer microstructure by an electric field has been studied intensively,[10–40] due to the possibility of tailoring the spatial anisotropy in block copolymer morphologies. Moreover, applications of an electric field are used to investigate the behavior of block copolymer materials near the ODT. For example, Thurn-Albrecht *et al.*[53] used the electric field to fabricate ultrahigh-density arrays of nanopores in a polymer matrix by removal of one component of an electric field aligned cylindrical microstructure. These regularly allocated nanopores are filled by a metal in order to produce continuous metal nanowires with well-defined properties and controlled sizes. Also, well-ordered block copolymer microdomains are used as the templates in a block copolymer lithography technique.[54] A lot of theoretical and experimental works have been devoted to bulk and thin copolymer films subjected to an electric field.

From the experimental side, the melt microdomain alignment in thin films was investigated in a number of studies.[23–32] Mansky *et al.* reported on a field-induced orientation in thin films of asymmetric poly(styrene-*block*-methyl methacrylate) diblock copolymer (PS-*b*-PMMA) melt with a cylindrical morphology.[23] Morkved *et al.*[24,25] examined the effect of an electric field on cylindrical microdomain orien-

[a)]Electronic mail: a.kyrylyuk@tue.nl

tation in thin films of asymmetric PS-*b*-PMMA melt. In their research it was shown that cylindrical microdomains were aligned parallel to the electric field with some defects. The electrode thickness was rather small, so that the influence of electrodes on a cylinder orientation was excluded. The competition between interfacial interactions and the applied electric field was inspected by Thurn-Albrecht *et al.*[26,27] Samples of asymmetric PS-*b*-PMMA melts with different thicknesses were subjected to electric fields of different strengths. They found that the threshold electric field strength must be exceeded to achieve a complete cylinder orientation parallel to the electric field direction.[26] The threshold field strength was found to be independent of the thickness of the sample. Depending on the field strength, the parallel or perpendicular cylinder alignment was observed. In Ref. 27, a strong orientation of the cylindrical microstructure parallel to the substrate surface under the influence of an external electric field was obtained. It was shown that cylindrical microdomains can be used to generate an array of ordered nanoscopic pores with well-controlled size, orientation, and structure.[27] In Ref. 28, Thurn-Albrecht *et al.* investigated the electric-field-induced orientation in a block copolymer melt with the copolymer in different initial states, using *in situ* small-angle x-ray scattering (SAXS). Beginning with a disordered copolymer, the electric field was found to orient composition fluctuations in the disordered state, leading to a preferred growth of well-aligned nuclei. Beginning with a microphase-separated copolymer where the cylindrical microdomains were oriented normal to the field, the domain orientation became unstable at high field strengths, and the microdomains reoriented in a piecewise manner.[28]

Thin film lamellar alignment was reported by Russell and co-workers.[29–32] The alignment of diblock copolymer melt microdomains by an electric field was found to be dependent on the segmental interaction between two blocks and the difference in the interfacial energies of each block with the substrate.[29] Complete alignment of the lamellar microdomains in the direction of the applied electric field was found only when the interactions of the blocks with the substrate were balanced. In all other cases, a mixed orientation of the microdomains was obtained. In Ref. 30, the dependence of the electric field alignment of a symmetric diblock copolymer (PS-*b*-PMMA) was studied as a function of film thickness using *in situ* small-angle neutron scattering (SANS) and transmission electron microscopy (TEM). With increasing film thickness, surface effects diminished with distance, and the applied field oriented the lamellar microdomains in the center of the film in the direction of the applied field. The results of this study indicated that the lamellae locally broke up and then are reformed.[30] The electric-field-induced orientations of ordered, symmetric poly(styrene-*block*-isoprene) diblock copolymer (PS-*b*-PI) and PS-*b*-PI-*b*-PS triblock copolymer melts were investigated in Ref. 31 by means of time-resolved SAXS. The scattering patterns showed contributions corresponding to a state of intermediate alignment with distinctly different peak shapes.[31] This indicated partial disordering of the copolymer during reorientation. The use of two orthogonal, external fields to control the orientation of lamellar microdomains in three dimensions in diblock copolymer thin films has been reported in Ref. 32. An elongational flow field was applied to obtain an in-plane orientation of the microdomains of the copolymer melt, and an electric field, applied normal to the surface, was used to further align the microdomains and, thereby, produce a near single-crystal texture.

From a theoretical perspective, the alignment of block copolymer microstructures in bulk was analyzed by Amundson *et al.*[10–12] They surveyed the weak segregation regime by minimizing the free energy of dielectric material. By this static analysis the lamellar and cylindrical morphologies were predicted as only existing in the presence of an external electric field. Different alignment mechanisms were considered. The theoretical model was supported by experimental investigations of lamellar alignment in the symmetric PS-*b*-PMMA sample. Onuki and Fukuda[13,14] studied the dynamics of undulation instability of lamellar structures in weak segregation limit. Also, they performed the numerical study of such instabilities in two-dimensional systems. Matsen[15] examined the stability of a lamellar layer of diblock copolymer in a strong electric field by means of self-consistent field theory (SCFT). Using SCFT, Lin *et al.*[16] and Tsori *et al.*[17] studied the structural changes of diblock copolymer melts in bulk due to an external electric field. The structure of diblock copolymer melts under a single external electric field or shear field, as well as under combined orthogonal external fields, was investigated by Feng and Ruckenstein[18] using cell dynamics algorithm. In these theories[10–18] orientation under an electric field is supposed to be caused by the electrostatic interactions of block copolymer microstructures and compositional fluctuations. A very different approach to the investigation of a microphase separation of block copolymers in an electric field was performed by Gurovich.[20–22] In this theory the polymer chains are aligned individually, and ordered phase appears from disorder already aligned by an electric field.

Most theoretical studies to examine thin film lamellar and cylindrical alignments in melts were carried out in the strong segregation limit. Pereira and Williams[33] addressed their study to lamellar alignment of a symmetric diblock copolymer melt thin film or bulk using a capacitor analogy. The phase diagram exhibiting parallel, perpendicular, and mixed alignment states was drawn up depending on electric field strength, surface interactions with different blocks, and distance between two identical flat bounding surfaces. Ashok *et al.*[34] took a similar approach by investigating both lamellar and cylindrical morphologies again in the strong segregation limit. Only parallel and perpendicular states were considered. The threshold field between these two alignment states was predicted to be dependent on a distance between electrodes, different from Pereira and Williams's finding. The transition between spherical and cylindrical morphologies and their stability in a diblock copolymer thin film in the intermediate segregation limit were studied by Matsen.[19] The limit of weak segregation, as well as strong segregation, in thin films has been considered by Tsori and Andelman.[35,36] In the strong segregation limit two critical electric fields for transitions between parallel, perpendicular, and mixed lamellar states were found. In the weak segregation limit one critical

electric field was calculated by minimizing the free energy. Below this critical field, the perfect parallel to the surfaces ordering has been predicted. The electric field just above the critical field gave the intermediate lamellar morphology, which was a superposition of parallel and perpendicular lamellae. The higher electric field resulted in perpendicular to the surface lamellae with residual small distortions. No mixed phases were predicted in the weak segregation regime.

In contrast with above-mentioned static theories, we investigated a more general case of dynamics of morphology alignment in confined films of diblock copolymer melts subjected to an electric field in the framework of dynamic density functional theory (DDFT). The theory used here is applicable in the weak and intermediate segregation limits. The confining surfaces (electrodes) and the electric field were chosen to align the lamellar microstructure in perpendicular directions. We quenched the homogeneous melt and applied the electric field and surface interactions simultaneously. The applied electric field aligns lamellar planes parallel to the electric field direction, whereas the surface field orients lamellae parallel to the surfaces, i.e., perpendicular to the electric field. Depending on the relative strength of the two competing field, the system exhibits a parallel or perpendicular orientation.

II. THEORY: THERMODYNAMICS AND EQUATIONS OF BLOCK COPOLYMER MORPHOLOGY DYNAMICS IN AN EXTERNAL ELECTRIC FIELD

We consider a block copolymer system consisting of different polymer blocks. Each part of a copolymer exhibits dielectric properties, and the whole system behaves as a simple dielectric material. In such a case it is possible to consider the electric field effects using a common theory of dielectrics in an external electric field. The electric field polarizes the medium and orients polar moments. Different constituents have different electric permittivities. Due to difference in permittivities of constituents, an applied field induces charges on surfaces between regions containing excess of one polymer component. The regions rich in one component and poor in others have different forms and sizes up to several tens of nanometers and always exist because of density fluctuations or macro- and microphase separations occurring in a system. The surface charges reduce the magnitude of an electric field within a dielectric sample. These electrostatic interactions contribute to the total energy of a block copolymer pattern.

The expression for the total free energy F of dielectric block copolymer sample, expressed as a volume integral over the field, generally reads as follows:[55,56]

$$F = F_0 - \frac{1}{8\pi}\int_V \varepsilon(\mathbf{r})|\mathbf{E}(\mathbf{r})|^2 d\mathbf{r}, \tag{1}$$

where F_0 is the free energy of the system in the absence of an electric field, $\mathbf{E}(\mathbf{r})$ is the electric field inside a sample, $\varepsilon(\mathbf{r})$ is the local electric permittivity of the material, and the integral extends over the volume V of the sample.

For calculating the electric field part of the free energy we have followed the method of Amundson *et al.*[11] They calculated the space-dependent electric field within the sample and associated free energy for the case of an incompressible system, where the one order parameter approximation is valid. For compressible systems considered here it is necessary to derive the dependence of electric field and free energy on order parameters for a multicomponent copolymer system with many order parameters, which in general case are independent.

Incompatibility of different blocks, adhesive and repulsive interactions with electrode surfaces or filler particles within a system, and diverse fluctuations result in different composition structures within a block copolymer sample. The composition structures and, associated with them, space-dependent local permittivity produce different patterns in an electric field. As a consequence, we have electrostatic contributions to the free energy depending on the composition pattern.

The fluctuations in the local permittivity tensor may arise from temporal and spatial fluctuations in the density (or concentration) and temperature. Usually, the fluctuations in the temperature $(\partial\varepsilon/\partial T)_\rho$ are much smaller than fluctuations in the density $(\partial\varepsilon/\partial\rho)_T$, and can thus be neglected.[57] As a result, we consider only fluctuations in the local permittivity tensor at constant temperature.

The anisotropic fluctuating part of the dielectric tensor is assumed to be much smaller than its isotropic part. Therefore, the anisotropic part of the electric polarizability tensor of a polymer is skipped. In addition, we assume that an electric field directly follows the time evolution of fluctuations, so that the time dependence of fluctuations can be neglected.

As a consequence, the local dielectric constant ε of a block copolymer melt is a scalar isotropic quantity. The permittivity is a function of the compositional pattern, and it is assumed to be expandable around the critical value of composition when the system is homogeneous. To describe composition patterns of a block copolymer system we use the complete set of compositional order parameters $\psi_I(\mathbf{r})$, which relate to concentration fields $\rho_I(\mathbf{r})$ as

$$\psi_I(\mathbf{r}) = \rho_I(\mathbf{r}) - \rho_I^0, \tag{2}$$

where index I denotes the component of a block copolymer; the order parameter $\psi_I(\mathbf{r})$ is equal to the deviation of the concentration $\rho_I(\mathbf{r})$ of one component of a diblock copolymer from the average value ρ_I^0.

We expand the dielectric constant to the first order in the compositional order parameters,

$$\varepsilon(\mathbf{r}) = \varepsilon^0 + \sum_I \varepsilon_I' \psi_I(\mathbf{r}), \tag{3}$$

where all derivatives $\varepsilon_I' \equiv \partial\varepsilon/\partial\psi_I$ are taken under conditions $\psi_I(\mathbf{r})=0$ (Taylor's expansion is about the homogeneous distribution of all components when $\rho_I(\mathbf{r})=\rho_I^0$), the sum is over all components, and ε^0 is the permittivity of the homogeneous state of a block copolymer material. The dielectric constant ε^0 also can be treated as a space-averaged dielectric constant of the sample.

Solving the Maxwell's equation

$$\nabla \cdot [\varepsilon(\mathbf{r})\mathbf{E}(\mathbf{r})] = 0 \tag{4}$$

in Fourier space gives us (see the Appendix) the anisotropic part of electrostatic contribution F_{el} to the free energy

$$F_{\mathrm{el}} = \frac{1}{64\pi^4}\frac{1}{\varepsilon^0}E_0^2\sum_{I,J}\varepsilon_I'\varepsilon_J'\int \psi_I(\mathbf{k})\psi_J(-\mathbf{k})\left(\frac{\mathbf{k}}{k}\cdot\mathbf{e}\right)^2 d\mathbf{k}, \tag{5}$$

where $k=|\mathbf{k}|$, $E_0=|\mathbf{E}_0|$ (the strength of the uniform applied field), and $\mathbf{e}$ is the unit vector along the direction of the external electric field.

In this derivation the effects of chain deformations on a microphase separation due to anisotropy of the electric polarizability tensor of monomers are neglected. In a model for block copolymers developed by Gurovich,[20–22] which is based on Leibler's random phase approximation (RPA) method,[58] an applied electric field polarizes the monomers, interacts with induced polar moments, and orients them. It has been shown by Onuki and Fukuda[13] that for most polymers the ratio of the strength of the electrostatic interaction in Gurovich's model and that of the induced dipolar interaction considered here is much smaller than unity. Hence, Gurovich's mechanism of interaction between an applied field and a nonionic block copolymer melt can be omitted.

To express the free energy F_0 of a block copolymer melt in the absence of an electric field we model the copolymer melt as a slightly compressible system in a mean-field environment.[59] Mean-field methods have been applied successfully to the description of equilibrium and dynamical properties of block copolymer melts.[15,19,37,38,58–60] We do not account for density fluctuations, which are important in the vicinity of the ODT.[58] Since we consider a block copolymer system in the intermediate segregation limit, far beyond the ODT, the application of a mean-field description is well justified. We considered a diblock copolymer melt of the volume V which contains n diblock copolymer Gaussian chains, each of length $N=N_A+N_B$. In such a system there are two concentration fields $\rho_A(\mathbf{r})$ and $\rho_B(\mathbf{r})$, two external potentials $U_A(\mathbf{r})$ and $U_B(\mathbf{r})$ conjugated to the concentration fields ρ_A and ρ_B, respectively, and two intrinsic chemical potentials $\mu_A(\mathbf{r})$ and $\mu_B(\mathbf{r})$. The type of A or B beads is marked by I. The bead index number is $l=1,\ldots,N$.

The free energy F_0 is the intrinsic free energy functional $F_0[\rho]$ of the system, and it has the following form:[3,60,61]

$$\begin{aligned} F_0[\rho] &= F^{\mathrm{id}}[\rho] + F^{\mathrm{nid}}[\rho] \\ &= -\beta^{-1}\ln\frac{\Phi^n}{n!} - \sum_I \int_V U_I(\mathbf{r})\rho_I(\mathbf{r})d\mathbf{r} \\ &\quad + \frac{1}{2}\sum_{I,J}\int_V\int_V \epsilon_{IJ}(|\mathbf{r}-\mathbf{r}'|)\rho_I(\mathbf{r})\rho_J(\mathbf{r}')d\mathbf{r}d\mathbf{r}' \\ &\quad + \sum_I \int_V\int_V \epsilon_{IS}(|\mathbf{r}-\mathbf{r}'|)\rho_I(\mathbf{r})\rho_S(\mathbf{r}')d\mathbf{r}d\mathbf{r}' \\ &\quad + \frac{\kappa_H\nu^2}{2}\int_V\left(\sum_I \rho_I(\mathbf{r}) - \sum_I \rho_I^0\right)^2 d\mathbf{r}, \end{aligned} \tag{6}$$

where $\beta^{-1}=k_BT$, κ_H is the Helfand's compressibility parameter, ν is the average volume of the statistical unit (the same for all beads), Φ is the intramolecular partition function for the ideal Gaussian chain in the external field U_I, $\epsilon_{IJ}(|\mathbf{r}-\mathbf{r}'|)=\epsilon_{JI}(|\mathbf{r}-\mathbf{r}'|)$ is a cohesive interaction between beads of type I at $\mathbf{r}$ and J at $\mathbf{r}'$, and $\epsilon_{IS}(|\mathbf{r}-\mathbf{r}'|)$ is a cohesive interaction parameter between a bead of type I and the surface. The first two terms in Eq. (6) comprise the entropic contribution of ideal Gaussian chains in a mean-field environment. The third and fifth terms account for the cohesive interactions between beads and the excluded volume interactions, respectively. The fourth term gives rise to the interaction of a polymer with surfaces and contributes only in the vicinity of the surface, which reveals the short-range nature of polymer interactions with hard filler objects.

The surfaces inside the system, which represent electrode surfaces of a real system, occupy the volume V^0. The constant concentration field ρ_S in Eq. (6) is defined as $\rho_S(\mathbf{r})=1$ if $\mathbf{r}\in V^0$ and $\rho_S(\mathbf{r})=0$ if $\mathbf{r}\in V/V^0$. All surfaces are supposed to have fixed stationary positions.

The relation between concentrations and the external potentials is given by a density functional

$$\rho_I[U](\mathbf{r}) = S(\mathbf{r})n\sum_{l=1}^{N}\delta_{Il}\,\mathrm{Tr}_c(\Gamma(\mathbf{R}_l)\delta(\mathbf{r}-\mathbf{R}_l)), \tag{7}$$

where δ_{Il} is a Kronecker delta function, $\mathbf{R}_l$ is the position of the lth bead, $S(\mathbf{r})$ is a surface field, and $\Gamma(\mathbf{R}_l)$ is the single-chain configuration distribution function

$$\Gamma(\mathbf{R}_l) = \frac{1}{\Phi}\exp\left[-\beta\left(H^G + \sum_{l=1}^{N}U_l(\mathbf{R}_l)\right)\right], \tag{8}$$

with the Gaussian chain Hamiltonian

$$H^G = \frac{3}{2\beta a^2}\sum_{l=2}^{N}(\mathbf{R}_l - \mathbf{R}_{l-1})^2. \tag{9}$$

Here, a is the Gaussian bond length parameter. A surface field $S(\mathbf{r})$ is defined as $S(\mathbf{r})=0$ for $\mathbf{r}\in V^0$ and $S(\mathbf{r})=1$ for $\mathbf{r}\in V/V^0$.

We assume that in the slowly relaxing polymeric system the interactions do not depend on the momenta. Therefore, the trace Tr_c is limited to the integration over the coordinates of one chain,

$$\mathrm{Tr}_c(\cdot) \equiv \frac{1}{\Lambda^{3N}}\int_{V^N}(\cdot)\prod_{l=1}^{N}d\mathbf{R}_l, \tag{10}$$

where Λ is a normalization factor (see Ref. 59).

A cohesive interaction parameter between beads ϵ_{IJ} has the same Gaussian kernel as an ideal Gaussian chain Hamiltonian,

$$\epsilon_{IJ}(|\mathbf{r}-\mathbf{r}'|) \equiv \epsilon_{IJ}^0\left(\frac{3}{2\pi a^2}\right)^{3/2}\exp\left[-\frac{3}{2a^2}(\mathbf{r}-\mathbf{r}')^2\right]. \tag{11}$$

The surface interactions ϵ_{IS} with diblock copolymer components have similar kernels.

A pair of the concentration fields ρ and the external potential fields U define a unique value of a free energy F_0 due

to the bijective relation between them. For every set of fields $\{U_I\}$ exists only one set of fields $\{\rho_I\}$. As a result of this, there is a unique inverse density functional $U_I[\rho]$.

The density functional is calculated via the following procedure (see Ref. 59 for details):

$$\rho_l(\mathbf{r}) \propto G_l(\mathbf{r})\sigma[G_{l+1}^{\mathrm{inv}}](\mathbf{r}), \tag{12}$$

where the set of once integrated Green's functions $G_l(\mathbf{r})$ and $G_l^{\mathrm{inv}}(\mathbf{r})$ are related by the recurrence formulas

$$\begin{aligned} G_l(\mathbf{r}) &= S(\mathbf{r})\exp[-\beta U_l(\mathbf{r})]\sigma[G_{l-1}](\mathbf{r}), \\ G_l^{\mathrm{inv}}(\mathbf{r}) &= S(\mathbf{r})\exp[-\beta U_l(\mathbf{r})]\sigma[G_{l+1}^{\mathrm{inv}}](\mathbf{r}), \end{aligned} \tag{13}$$

with $G_0(\mathbf{r})=G_{N+1}^{\mathrm{inv}}(\mathbf{r})=1$. The linkage operator $\sigma=\sigma[f](\mathbf{r})$ is interpreted as a convolution with a Gaussian kernel,

$$\sigma[f](\mathbf{r}) \equiv \left(\frac{3}{2\pi a^2}\right)^{3/2}\int_V \exp\left[-\frac{3}{2a^2}(\mathbf{r}-\mathbf{r}')^2\right]f(\mathbf{r}')d\mathbf{r}', \tag{14}$$

with the normalization $\sigma[1](\mathbf{r})=1$. The employed Green's propagator method using path integral formalism to calculate the density functional (7) gives an exact answer and yields the realistic dynamics of concentration field evolution in time.

The intrinsic chemical potentials $\mu_I(I=A,B)$, defined as the functional derivative of the free energy F with respect to concentration fields ρ_I, consist of following two parts:

$$\mu_I(\mathbf{r}) \equiv \frac{\delta F[\rho]}{\delta\rho_I(\mathbf{r})} = \mu_I^0(\mathbf{r}) + \mu_I^E(\mathbf{r}), \tag{15}$$

where chemical potentials $\mu_I^0(\mathbf{r})$ in the absence of an applied electric field have the form

$$\begin{aligned} \mu_I^0(\mathbf{r}) = &- U_I(\mathbf{r}) + \sum_J \int_V \epsilon_{IJ}(|\mathbf{r}-\mathbf{r}'|)\rho_J(\mathbf{r}')d\mathbf{r}' \\ &+ \kappa_H\nu^2\sum_J \rho_J(\mathbf{r}). \end{aligned} \tag{16}$$

The electrostatic part of the chemical potential $\mu_I^E(\mathbf{r})$ has a simple form in the Fourier space. Using Eq. (5) one finds the following expressions for the Fourier transforms $\mu_I^E(\mathbf{k})$ of chemical potentials:

$$\begin{aligned} \mu_A^E(\mathbf{k}) &= \frac{1}{4\pi}\frac{1}{\varepsilon_0}E_0^2[(\varepsilon_A')^2\psi_A(-\mathbf{k}) + \varepsilon_A'\varepsilon_B'\psi_B(-\mathbf{k})]\left(\frac{\mathbf{k}}{k}\cdot\mathbf{e}\right)^2, \\ \mu_B^E(\mathbf{k}) &= \frac{1}{4\pi}\frac{1}{\varepsilon_0}E_0^2[(\varepsilon_B')^2\psi_B(-\mathbf{k}) + \varepsilon_A'\varepsilon_B'\psi_A(-\mathbf{k})]\left(\frac{\mathbf{k}}{k}\cdot\mathbf{e}\right)^2. \end{aligned} \tag{17}$$

Here, the electrostatic parts of chemical potentials for a two-component diblock copolymer system are made explicit. All previous equations were written for multicomponent systems, containing, in principle, any number of components. Further calculations will be derived for a two-component copolymer melt.

Now we introduce the dynamic equations to describe the diffusive dynamics of the concentration fields. We examine the problem in the intermediate segregation limit. Since the considered length scale is much larger than the characteristic end-to-end distance of chains, we can use dynamic equations in the same form as those for critical fluids.[62]

Notice that we do not consider any hydrodynamic interactions. Under these conditions of no hydrodynamic interactions the phase separation is described by the modified time-dependent Ginzburg-Landau equation. The model put in practice is a generalization of model **B** according to Hohenberg and Halperin.[62] We study the situation in which the Onsager coefficients are local and constant. For this type of a coarse-grained model it is legitimate to apply the Langevin equations in the diffusion form

$$\frac{\partial\rho_I(\mathbf{r})}{\partial t} = M\Delta\mu_I(\mathbf{r}) + \eta_I(\mathbf{r},t), \tag{18}$$

where M is the mobility coefficient and $\eta_I(I=A,B)$ are the thermal noise fields, distributed according to a fluctuation-dissipation theorem (FDT),[59,63,64]

$$\begin{aligned} &\langle\eta_I(\mathbf{r},t)\rangle = 0, \\ &\langle\eta_I(\mathbf{r},t)\,\eta_J(\mathbf{r}',t')\rangle = -2\beta^{-1}\delta_{IJ}M\delta(t-t')\nabla_{\mathbf{r}}\cdot\delta(\mathbf{r}-\mathbf{r}')\nabla_{\mathbf{r}'}. \end{aligned} \tag{19}$$

For the sake of simplicity, mobility coefficients are chosen to be identical for all components.

Since we have the simple expressions for the electrostatic parts of the chemical potentials (17) in the Fourier space, it is expedient to make a Fourier transformation of Eq. (18). Finally, with the aid of Eqs. (15) and (17), after making an inverse Fourier transformation of the obtained equations, the stochastic diffusion equations describing the mesoscopic evolution of the concentration fields are expressed as

$$\begin{aligned} \frac{\partial\rho_A(\mathbf{r})}{\partial t} &= M\Delta\mu_A^0(\mathbf{r}) + M\frac{1}{4\pi}\frac{1}{\varepsilon^0}E_0^2 \\ &\quad\times\left[(\varepsilon_A')^2\frac{\partial^2\rho_A(\mathbf{r})}{\partial z^2} + \varepsilon_A'\varepsilon_B'\frac{\partial^2\rho_B(\mathbf{r})}{\partial z^2}\right] + \eta_A(\mathbf{r},t), \\ \frac{\partial\rho_B(\mathbf{r})}{\partial t} &= M\Delta\mu_B^0(\mathbf{r}) + M\frac{1}{4\pi}\frac{1}{\varepsilon^0}E_0^2 \\ &\quad\times\left[(\varepsilon_B')^2\frac{\partial^2\rho_B(\mathbf{r})}{\partial z^2} + \varepsilon_A'\varepsilon_B'\frac{\partial^2\rho_A(\mathbf{r})}{\partial z^2}\right] + \eta_B(\mathbf{r},t). \end{aligned} \tag{20}$$

While deriving these equations we have used relation (2) between the compositional order parameters and the field of concentrations. Equations (20) were written down on the assumption that external electric field is applied parallel to the z axis of the laboratory coordinate system, $\mathbf{e}=\mathbf{e}_z$.

To estimate the values $\varepsilon_I(I=A,B)$, which define the change in a dielectric constant with composition changes, we suppose the linear dependence of the dielectric constant of a binary system on component concentrations,

$$\varepsilon = \nu\rho_A\varepsilon_A + \nu\rho_B\varepsilon_B, \tag{21}$$

where ε_A and ε_B are the dielectric constants of two pure copolymer components A and B, respectively. This linear approximation for a dielectric constant is a quite good one as long as the variations of concentration fields are small, and

there is a low difference in the dielectric constants of two components.

Furthermore, since we consider only slightly compressible systems one can use the following dynamic constraint:

$$\nu^{-1} = \rho_A(\mathbf{r}) + \rho_B(\mathbf{r}). \tag{22}$$

The volume ν occupied by one statistical unit is considered to be a constant. Note that the molecular volume ν is a constant only for incompressible systems. In a case of slightly compressible systems, which we investigated, it is convenient to put it in practice to evaluate approximate values, in order of magnitude.

Within the framework of these approximations the values ε_I' are easily calculated as

$$\varepsilon_A' = -\varepsilon_B' = \nu(\varepsilon_A - \varepsilon_B). \tag{23}$$

The absolute values of derivatives ε_A' and ε_B' are the same and will be defined below as ε', $\varepsilon' = |\varepsilon_A'| = |\varepsilon_B'|$.

In the present study we consider only a symmetric diblock copolymer melt (the volume fractions of components are half). From Eqs. (21) and (22) one can calculate the space-averaged dielectric constant ε^0 of a symmetric diblock copolymer melt,

$$\varepsilon^0 = \frac{\varepsilon_A + \varepsilon_B}{2}. \tag{24}$$

For slightly compressible diblock copolymer melts Eqs. (20) turn into a set of two coupled equations

$$\frac{\partial \rho_A(\mathbf{r})}{\partial t} = M\Delta\mu_A^0(\mathbf{r}) + M\frac{1}{2\pi}\frac{(\varepsilon')^2}{\varepsilon^0}E_0^2\frac{\partial^2\rho_A(\mathbf{r})}{\partial z^2} + \eta_A(\mathbf{r},t),$$
$$\frac{\partial \rho_B(\mathbf{r})}{\partial t} = M\Delta\mu_B^0(\mathbf{r}) + M\frac{1}{2\pi}\frac{(\varepsilon')^2}{\varepsilon^0}E_0^2\frac{\partial^2\rho_B(\mathbf{r})}{\partial z^2} + \eta_B(\mathbf{r},t), \tag{25}$$

which we already used in Ref. 37 to investigate the lamellar alignment in bulk.

In the direction perpendicular to the electrode surfaces we use rigid-wall boundary conditions, fulfilled by allowing no flux through the surfaces[3,60,61]

$$\nabla\mu_I \cdot \mathbf{n}_S = 0, \tag{26}$$

where $\mathbf{n}_S$ is the normal to the surfaces, directed in this particular study along the z axis of the laboratory coordinate system, $\mathbf{n}_S = \pm\mathbf{e}_z$. The rigid-wall boundary conditions in this direction are also employed for the noise η_I. In all other directions periodic boundary conditions are applied.

III. NUMERICAL PROCEDURE AND CHARACTERISTICS OF AN ORIENTATIONAL ORDER

Equations of motion (25) can be integrated efficiently on a cubic grid by a Crank-Nicolson (CN) scheme, combined with the steepest descent method for an iteration of the inner loop.[59,63,64] After discretizing the dynamic equations (25) we obtain the following dimensionless CN equations for each component I (A or B):

$$\theta_I^k - \omega_1\Delta\tau z_{Ip}^k - \omega_2\Delta\tau B f_{Ip}^k = \theta_I^{k-1} + (1-\omega_1)\Delta\tau z_{Ip}^{k-1} + (1-\omega_2)\Delta\tau B f_{Ip}^{k-1} + \eta_{Ip}^{k-1}. \tag{27}$$

Here, η_{Ip}^{k-1} is the numerical noise, applied at each time step and distributed according to FDT; z_p^k and f_p^k denote the discretized diffusion parts at time k and cubic grid position p,

$$z_p = \sum_\alpha \sum_q d_\alpha [D_\alpha D_\alpha]_{pq}\phi_{Iq},$$
$$f_p = \sum_\alpha \sum_q d_\alpha [D_\alpha D_\alpha]_{pq}\theta_{Iq}. \tag{28}$$

D_α is the grid-restricted half-point discretized gradient operator in grid direction α.[59,63,64] All variables are dimensionless: dimensionless concentrations $\theta_I \equiv \nu\rho_I$, intrinsic chemical potentials $\phi_I \equiv \beta\mu_I^0$, time $\tau \equiv \beta^{-1}\nu M h^{-2} t$, electric field parameter B,

$$B \equiv \beta\nu^{-1}\frac{1}{2\pi}\frac{(\varepsilon')^2}{\varepsilon^0}E_0^2. \tag{29}$$

ω_1 and ω_2 are the CN parameters. In our simulations $\omega_1 = \omega_2 = 0.5$, and dimensionless time step $\Delta\tau \equiv \beta^{-1}\nu M h^{-2}\Delta t = 0.5$, where h is the mesh size of the physical grid.

We investigate the behavior of a symmetric diblock copolymer melt represented by a model diblock copolymer A_8B_8. The cubic grid is $L\times L\times L$ ($L=32$). For all simulations the dimensionless parameters have been chosen (see details in Refs. 59 and 63): The noise scaling parameter $\Omega \equiv \nu^{-1}h^3 = 100$. The grid parameter $d \equiv ah^{-1} = 1.1543$. The compressibility parameter $\kappa_H' \equiv \beta\kappa_H\nu = 30$. In the numerics we have three dimensionless exchange parameters $\beta\epsilon_{AB}^0/\nu$ and $\beta\epsilon_{AA}^0/\nu = \beta\epsilon_{BB}^0/\nu = 0.0$ (blocks of the same type do not interact). The mobility coefficient is related to the diffusion coefficient D as $D = \beta^{-1}\nu M$. The interaction parameters between blocks and the electrode surfaces $\beta\epsilon_{AS}^0/\nu$ and $\beta\epsilon_{BS}^0/\nu$ are different in different simulations. Notice that dimensionless parameters allow us to apply the results to different systems.

The dimensionless electric field parameter B is actually the ratio of the anisotropic part of the electrostatic energy (5) to the thermal energy β^{-1}, and it can be approximately expressed for slightly compressible symmetric diblock copolymer melts as

$$B = \frac{1}{\pi}\beta\nu\frac{(\varepsilon_A - \varepsilon_B)^2}{\varepsilon_A + \varepsilon_B}E_0^2. \tag{30}$$

A scaling analysis of the free energy and the dynamic equations shows that the relevant parameter governing the electric field effect is BN, similar to effective interaction parameter χN between different blocks (χ is the Flory-Huggins parameter).[37] All simulations with these scaled effective parameters give the same outcome. For a typical experimental system, $N\sim 10^5$ monomers, $\beta\sim 10^{21}$ J^{-1}, $\nu\sim 10^{-28}$ m^{-3} (molecular size), $E_0\sim 10^6$ V/m, $(\varepsilon_A-\varepsilon_B)^2/\pi(\varepsilon_A+\varepsilon_B)\sim 1$ (for example, $\varepsilon_{PS}=2.55$ and $\varepsilon_{PMMA}=3.78$),[12] and hence $BN\sim 10^{-1}$.[37] In our simulations we use $BN=0.32$.

The kinetics of the phase separation is monitored by the volume-averaged order parameter P, defined as

$$P \equiv \langle \theta^2 - (\theta^0)^2 \rangle_V = \frac{\nu^2}{V} \sum_I \int_V [\rho_I^2(\mathbf{r}) - (\rho_I^0)^2] d\mathbf{r}. \tag{31}$$

The order parameter P, which is the mean-squared deviation from homogeneous state, cannot be used to depict orientational changes in a block copolymer microstructure. The order parameter P is a reliable quantity to monitor the grade of a phase separation of different blocks. It reflects changes in the grade of phase demixing and does not capture the alignment kinetics of lamellae already phase separated, as changing of a lamellar orientation due to influence of an electric field or surfaces does not involve a significant demixing of copolymer species.

To characterize the alignment process of lamellar pattern we use the orientational order parameter P_2 for two-dimensional (2D) and three-dimensional (3D) systems according to

$$P_2^{(2D)} = 2\langle \cos^2 \gamma \rangle - 1, \tag{32a}$$

$$P_2^{(3D)} = \tfrac{3}{2}\langle \cos^2 \gamma \rangle - \tfrac{1}{2}, \tag{32b}$$

where $\langle \cos^2 \gamma \rangle$ is the squared cosine of the angle γ between the unit vector $\mathbf{n}(|\mathbf{n}|=1)$ normal to the lamella and the unit vector $\mathbf{e}_z$ of an external electric field; the angular brackets $(\cdots)$ denote an averaging over the probability distribution function for the normals of the lamellae. By construction, for random orientation of lamellae $\langle \cos^2 \gamma \rangle$ is 1/2 in 2D and 1/3 in 3D and hence P_2 is zero.

In the 2D case $P_2^{(2D)}$ ranges between -1 and 1. For perfect perpendicular alignment of the lamellae, i.e., alignment along the direction of an external electric field ($\gamma=90°$), $P_2^{(2D)}=-1$. For perfect parallel alignment ($\gamma=0°$), i.e., all lamellae are parallel to the surfaces (two parallel electrodes), $P_2^{(2D)}=1$.

In the 3D case $P_2^{(3D)}$ ranges between -0.5 and 1. The value $P_2^{(3D)}=-0.5$ corresponds to a perfect perpendicular alignment where normals of all lamellae are directed parallel to the electrode surfaces, i.e., all lamellae are oriented parallel to the applied electric field. The value $P_2^{(3D)}=1$ refers to a perfect parallel alignment with all lamellae planes lying parallel to the planar electrode surfaces.

Increasing the orientational order parameter means that at this stage the alignment by surfaces prevails over the electric field alignment. Decreasing P_2 corresponds to the domination of alignment by an electric field. If P_2 takes negative values, the lamellae are preferably oriented in the direction of an electric field. Positive values of P_2 indicate that there are more regions containing lamellae parallel to the surfaces. It reveals the domination of electric field over the surface effects.

The orientational order parameter P_2 is a relevant parameter to monitor the time evolution of orientational changes in a block copolymer microstructure. However, one must note that P_2 is only the second moment of the whole orientational distribution of lamellae normals, and its averaged value would correspond to different orientational distributions. In principle, to distinguish these distributions one needs to use higher moments of total distribution, and it can be that all moments would be necessary for a complete description of orientations. But for block copolymer systems to explore mesophase orientations and to draw surface and electric field alignments, it is enough to evaluate the second moment P_2 displaying the rate and type of alignment.

To evaluate the orientational order parameter P_2 via the concentration distributions, we suppose that the normal direction to the lamellae planes in 3D or lamellae stripes in 2D is the direction of a steepest change of concentrations. The assumption that lamellae normals coincide with the gradient direction is similar to an approximation of lamellae as isosurfaces in 3D (or as isolines in 2D) of a constant concentration. By definition, this means that the normal direction coincides with the direction of the gradient of concentration,

$$\mathbf{n} = \frac{\nabla \rho_A}{|\nabla \rho_A|}. \tag{33}$$

For specificity, we have taken the concentration of the A component of a diblock copolymer melt (using the concentration of the B component yields the same result). This gives the expression for $\cos \gamma$ as

$$\cos \gamma = \frac{\nabla_z \rho_A}{|\nabla \rho_A|}. \tag{34}$$

Substituting Eq. (34) into Eqs. (32a) and (32b), and using the relation $|\nabla \rho_A|^2 = (\nabla_x \rho_A)^2 + (\nabla_y \rho_A)^2 + (\nabla_z \rho_A)^2$ (or a similar relation in 2D), one easily obtains the required expressions for the orientational order parameter,

$$P_2^{(2D)} = \left\langle \frac{(\nabla_z \rho_A)^2 - (\nabla_x \rho_A)^2}{(\nabla_z \rho_A)^2 + (\nabla_x \rho_A)^2} \right\rangle_V, \tag{35a}$$

$$P_2^{(3D)} = \left\langle \frac{(\nabla_z \rho_A)^2 - \frac{1}{2}[(\nabla_x \rho_A)^2 + (\nabla_y \rho_A)^2]}{(\nabla_z \rho_A)^2 + (\nabla_x \rho_A)^2 + (\nabla_y \rho_A)^2} \right\rangle_V. \tag{35b}$$

Here, we replaced the averaging over the probability distribution function by spatial averaging over the volume of a sample, assuming that it does not give an essential error in calculations.

The spatial anisotropy of a block copolymer microstructure can also be displayed with the help of the set of parameters

$$Q_{\alpha\beta} = \langle \nabla_\alpha \rho_A \nabla_\beta \rho_A \rangle_V \quad (\alpha, \beta = x, y, z; \alpha \neq \beta), \tag{36}$$

which are related to the stress tensor due to domains.[65–67] Again, for specificity, we have taken the concentration of the A component. These anisotropy factors $Q_{\alpha\beta}$ represent the domain contribution to the stress tensor arising from the composition inhomogeneities; they do not represent the contribution due to changes in chain conformations. The time evolution of anisotropy factors $Q_{\alpha\beta}$, containing the z direction of an applied electric field, characterizes the growth of microdomains and deformations in a distorted by the electric field morphology. It also illustrates the alignment kinetics of a copolymer microstructure. If all lamellae are perfectly aligned parallel to the z direction of the external electric field, the factors $Q_{\alpha z}=0$. The homogeneous structure corresponding to the situation of no phase separation in a system (domain interfaces have not been formed yet) gives all pa-

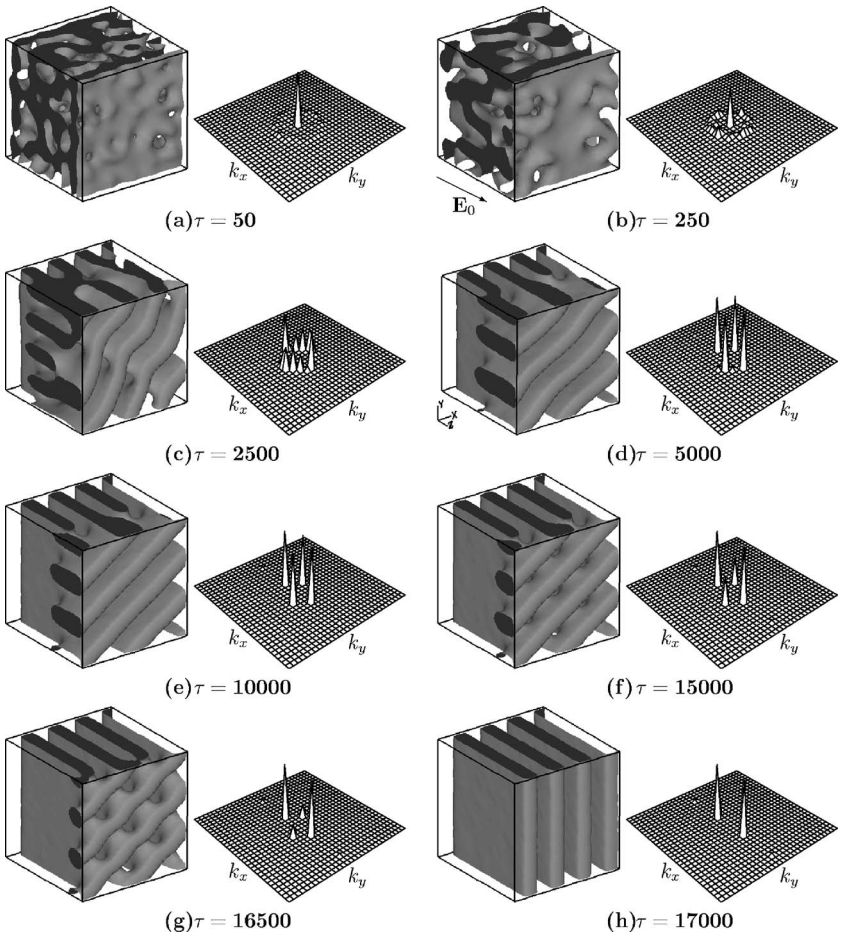

FIG. 1. Isosurface representation of a symmetric A_8B_8 diblock copolymer melt for $\nu\rho_A=0.5$ and the z projection of the 3D structure factor $S(\mathbf{k})$ at different dimensionless times τ. The surface related interaction parameter is $\beta\epsilon^0_{AS}/\nu=0.7$ $(\beta\epsilon^0_{BS}/\nu=0.0)$, corresponding to the adsorption energy $0.28k_BT$ per statistical unit.

rameters $Q=0$. In the 2D case the set of parameters Q is reduced to one anisotropy factor Q_{xz}.

IV. RESULTS AND DISCUSSION

In the present study, we consider only 3D systems of a model symmetric diblock copolymer melt A_8B_8. In order to depict different final morphologies and alignment kinetics depending on competition between electric field and surface interactions, we have performed a set of simulations with different surface interaction parameters $\beta\epsilon^0_{AS}/\nu(\beta\epsilon^0_{BS}/\nu=0.0)$. It means that bounding electrode surfaces are selective for copolymer blocks: surfaces are indifferent to B blocks and interact with A blocks. The situation of two identical parallel surfaces is considered. The electric field parameter $BN=0.32$ was fixed for all simulations. The interaction parameters between different blocks of a copolymer melt were also kept to be constant for all simulations, and they have been chosen to be $\beta\epsilon^0_{AA}/\nu=\beta\epsilon^0_{BB}/\nu=0.0$ and $\beta\epsilon^0_{AB}/\nu=3.0$, so that $\chi N\simeq 19.3$. The cubic grid is $32\times32\times32$. We quenched the homogeneous melt and applied the electric field and surface interactions simultaneously.

In Fig. 1 results are shown for the surface related interaction parameter $\beta\epsilon^0_{AS}/\nu=0.7$ (positive value of this parameter corresponds to repulsion between A block and surface), corresponding to the adsorption energy of $0.28k_BT$ per statistical unit. Note that this adsorption energy is above the critical surface interaction ($0.14k_BT$ for this particular system) below which the equilibrium lamellar morphology in the absence of an electric field would be perpendicular to the surfaces because of entropic effects.[38] In the present study, the surface selectivity is always larger than its critical value, so that the equilibrium lamellar morphology in the absence of an electric field would be parallel. From Fig. 1 one can trace the evolution of lamellae pattern and the z projection of the 3D structure factor $S(\mathbf{k})=\langle|\rho_A(\mathbf{k})|^2\rangle$. Figure 1(a) shows a not-yet-phase-separated microstructure at a very early time. One can clearly observe that near the surface one layer starts to form. This parallel to the surface layer is highly deformed, with many holes, because of a relatively small interaction with surfaces. The presence of two parallel to the surface layers gives two reflections into a scattering pattern, which are projected to one sharp central peak in the k_xk_y plane. The regions inside a film, quite far from the electrode surfaces, contain still growing lamellae locally correlated but globally randomly oriented somewhat similar to a picture of phase separation in bulk. The corresponding scattering function shown in the k_xk_y plane is an isotropic ring. The influence of an electric field is not visible at this level of phase separation. Figure 1(b) represents the later stage in the evolution of a still-phase-separating system. At this stage, formed earlier lamellar layers parallel to the surfaces are hugely perforated with no regularity, but they remain to be present. It is reflected in a scattering pattern: the central peak due to preferential surface alignment is still present, but the intensity of the peak decreases. A decrease of the intensity of the central peak is affected by the electric field influence. The effect of

an electric field is also seen from the transformation of isotropic ring in the $k_x k_y$ plane to the anisotropic ringlike pattern with very weak peaks corresponding to the lamellae, which start to grow in the electric field direction. The stage of complete prevalence of an electric field alignment over a surface alignment is shown in Fig. 1(c). The lamellae parallel to the surfaces were destroyed by the electric field. This corresponds to complete annihilation of the central peak in the z projection of the 3D structure factor. The mechanism of destruction of parallel lamellae is via the propagation of holes in lamellae [see Figs. 1(a) and 1(b)] into a striped pattern [Fig. 1(c)]. A structure shown in Fig. 1(c) consists of three coexisting lamellae clusters (grains) with lamellae parallel to the electric field, but oriented differently, perpendicular, to the electric field xy plane. An accompanied scattering pattern demonstrates four pairs of sharp Bragg peaks related to these clusters. One of the pairs of peaks corresponds to the uniformly oriented necks between lamellae of one of the clusters. The last lamellae cluster is highly undulated. The reason of such undulations is because this cluster tries to match the orientation of lamellae in a previous cluster. Upon three-cluster formation, an annihilation of a middle cluster occurs [see Fig. 1(d)]. The corresponding four distinct peaks in a structure factor confirm the coexistence of two lamellae clusters. The intensity of these peaks increased due to enlargement of the clusters. Two peaks have small satellite peaks which can also be treated as broadening of the peaks due to residual lamellae undulations. The amplitude of undulations slowly decreases throughout the morphological evolution until two coexisting clusters of straight lamellae become apparent [see Fig. 1(e)]. The presence in a system of two twisted, with respect to each other, clusters of perpendicular (parallel to the electric field) lamellae is not likely due to additional interfacial interactions between clusters. The grain boundary region between the two lamellae, which can be treated as a surface, the so-called intermaterial dividing surface (IMDS), costs an energy to a system. This surface is a defect in the microstructure, and it is thermodynamically unstable. There are several possibilities to remove a defect and to align a microstructure. The whole lamellae cluster can start turning to coincide the orientation of a neighboring cluster. This rigid-body-like mechanism of domain orientation involves great energy and is very unlikely. Another mechanism of selective disordering consistent with a melting of lamellae in unfavorable orientations and reformation of lamellae in preferable orientations is also very unlikely based on energetic arguments.[10–12] The most convenient mechanism of mesophase reorientation in thin films conforms to defect movement, which we already observed for bulk systems.[37] With regard to the monitored situation here, the IMDS moves in the direction of an electric field, as it is shown in Figs. 1(d)–1(g), until only one set of perpendicular lamellae survives [Fig. 1(h)]. While moving a boundary between clusters a volume fraction of one cluster increases with the decrease of another one. The corresponding scattering peaks change their intensity. From Figs. 1(d)–1(g) one can see the evident decrease of intensity of two peaks related to the cluster containing declined, with respect to box planes, lamellae. Such changes in a structure factor can be experimentally observed with the help of small-angle x-ray scattering (SAXS) or neutron scattering (SANS) measurements. The final morphology in Fig. 1(h) consists of perfect perpendicular lamellae. A z projection of the 3D structure factor exhibits two strong first order Bragg peaks even with visible peaks of second order and confirms a perfect lamellae alignment in the applied electric field direction.

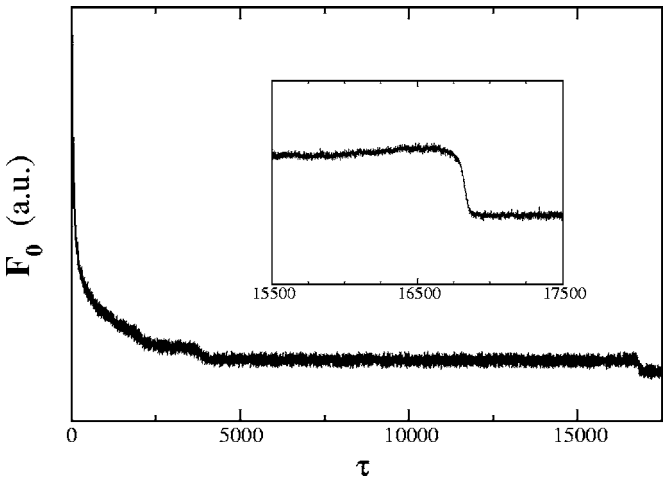

FIG. 2. The part F_0 of the total free energy of a diblock copolymer as a function of time τ for the surface related interaction parameter $\beta\epsilon_{AS}^0/\nu = 0.7$.

Now, we will clarify a driving force for moving a boundary between lamellae grains shown in Figs. 1(d)–1(g). From the evolution of the defect structures, we calculated the speed of boundary movement which remains constant during the reformation of lamellar microstructure, except in the initial stage of creation of this grain boundary [see Fig. 1(c)] and that of its disappearance [Fig. 1(g)]. The transversal motion of the defect structure of one cell in the system takes more than 10^3 time units, while the boundary passes the distance approximately equal to ten grid points. As the radius of gyration R_g of the polymers is about four grid points and one unit of time is smaller than the polymer relaxation time, this means that the polymer is in quasiequilibrium with respect to the defect structure. The anisotropic diffusion processes at the IMDS propel the motion of the surface. A relocation of the surface is not affected by an electric field. At least, the influence of an electric field on boundary movement is too small to be observed. The driving force of grain boundary movement at this very late stage of almost completely aligned lamellae in the direction of an applied field is a thermodynamic force $\nabla\mu_I^0$ related to part F_0 of the total free energy F of the sample without the electrostatic contribution F_{el}.

The changes in a free energy F_0 can be observed from Fig. 2. Figure 2 shows that while moving the cluster dividing surface there is no significant change (except thermal fluctuations) in the energy of the system. After the annihilation of the boundary nearly at $\tau = 16\,750$ the free energy F_0 drops down and reaches the lowest level, as shown in the inset of Fig. 2. Thus, the small energetic difference between the lamellar structures with and without a grain boundary is the driving force for the annihilation of grain boundaries. Note that in the vicinity of boundary disappearance, the free en-

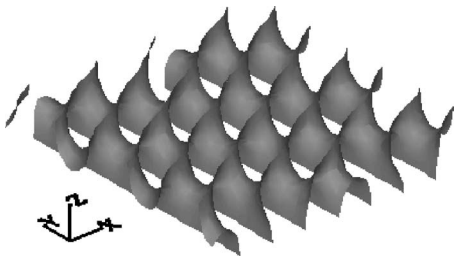

FIG. 3. The enlarged part of the two-cluster morphology shown in Fig. 1(e) containing the region of cluster dividing surface (the z position ranges between $z=17$ and $z=23$). The region exhibits a doubly periodic array of saddle surfaces.

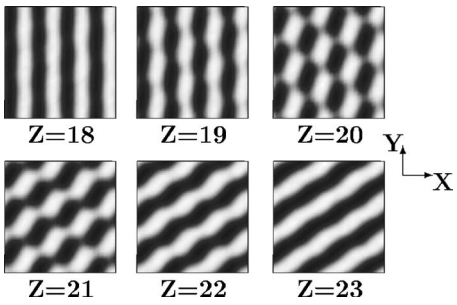

FIG. 4. The morphology scans through the region of cluster dividing surface in the same ranges, as shown in Fig. 3. The morphologies shown are xy orthoslices of two-cluster morphology from Fig. 1(e) at different z positions. The regions containing more A blocks are colored black with linear gray scale of the density $\nu\rho_A$ from 0.0 (black) to 1.0 (white).

ergy F_0 slightly increases due to small lamellae undulations shown in Fig. 1(g), leading to additional interfacial interactions. Figure 2 also illustrates the reduction of the part of the free energy F_0, related to the removal of the interfaces between $\tau=2500$ and $\tau=5000$ [see Figs. 1(c) and 1(d)] due to annihilation of one lamellae cluster, disappearing of necks, and suppression of lamellae undulations.

A peculiar effect is the shape of the surface between two lamellae clusters [Figs. 1(d)–1(g)]. In order to lower the energy, a system tends to minimize the surface area. In Fig. 3 the cropped morphology of Fig. 1(e) containing the region of the cluster dividing surface (the z position ranges between $z=17$ and $z=23$) at time $\tau=10\,000$ is shown at a different view angle. As can be seen from Fig. 3, this region consists of a doubly periodic array of saddle surfaces, similar to the Scherk's first surface twist boundary morphology.[68] In our case, this twist grain boundary (TGB) structure approximates a minimal surface with respect to minimization of total free energy F of a block copolymer sample in an electric field. The minimal surfaces, which we observed in the present study, allow a diblock copolymer lamellar phase to exclude unfavorable polymer chain conformations. The minimal surfaces have been experimentally observed to form in layers of block copolymers.[69,70] In the present paper, we do not discuss in detail the structure and motion of the TGB but rather concentrate on the electric-field-induced alignment of a diblock copolymer melt. A detailed analysis of the morphology of the TGB and its dynamics was made in our earlier paper,[40] in which the results on the structure of the TGB are compared to experiments of Gido *et al.*[69] and Gido and Thomas.[70]

The IMDS of the twist boundary morphology between two lamellae clusters at $\tau=10\,000$ [the same morphology as in Figs. 1(c) and 3] can be better seen in Fig. 4, in which the morphology scans through the neighboring xy planes are performed. In Fig. 4 one can observe all intermediate lamellar morphologies from one cluster of straight lamellae to another. These doubly periodic lamellae morphologies, obtained by cutting the microstructure at different positions of a dividing surface, look different and can help to indicate the presence of saddle surfaces in a microstructure for transmission electron microscopy (TEM) or scanning electron microscopy (SEM) measurements.

The evolution of lamellae orientations can be more quantitatively characterized by the orientational order parameter P_2 shown in Fig. 5. During the nucleation of lamellar microdomains the surface-driven alignment prevails over the electric field alignment, as can be seen from the sharp increase of the orientational order parameter (we use an inverted vertical axis for the orientational order parameter) until $\tau\simeq 50$. Inserting surfaces into a system induces order in the block copolymer microstructure and speeds up microphase separation. After $\tau\simeq 50$ an electric field starts to destroy a surface ordering, consistent with the decrease of P_2. At $\tau\simeq 400$ the order parameter takes the zero value, which corresponds to the competition of two effects. Then, the electric field effect prevails and the orientational order parameter smoothly decreases until it reaches the value $P_2\simeq -0.43$ close to its minimum -0.5, corresponding to perfectly aligned lamellae along the electric field. Because of the residual surface effects in the vicinity of the electrode surfaces the orientational order parameter did not reach its minimum -0.5. The disappearance of the IMDS between two lamellae clusters at $\tau\simeq 16\,750$ results in a jump in the order parameter. The region of $\tau=5000-15\,000$ shows a small decrease in P_2. An in significant change in the orientational order parameter during a boundary movement within these ranges is consistent with the small orientational transformations of a structure. The IMDS with a profile shown in Figs. 3 and 4 migrates in the z direction of the applied field, but the form of the profile does not change.

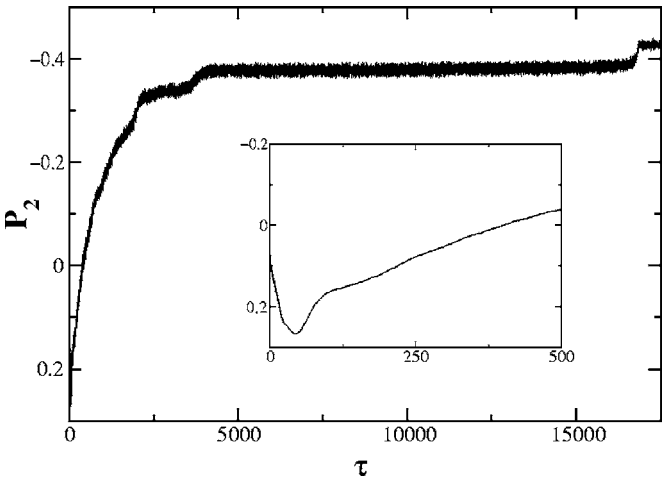

FIG. 5. Evolution of the orientational order parameter P_2 corresponding to the morphological transformations shown in Fig. 1. The surface related interaction parameter is $\beta\epsilon_{AS}^0/\nu=0.7$.

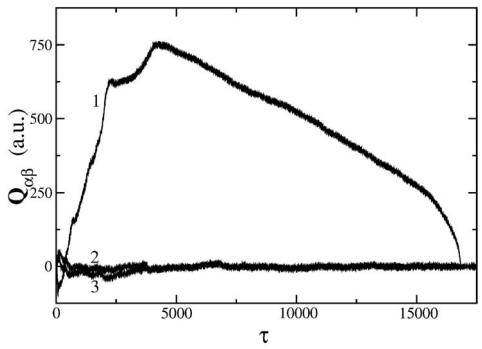

FIG. 6. The time evolution of stresses in the morphology $Q_{\alpha\beta}$ due to domains Q_{xy} (curve 1), Q_{xz} (curve 2), and Q_{yz} (curve 3).

The time evolution of stresses in the morphology $Q_{\alpha\beta}$ due to domains is shown in Fig. 6. The sharp increase of Q_{xz} (curve 2 in Fig. 6) and Q_{yz} (curve 3) as well as the decrease of Q_{xy} (curve 1) until $\tau \simeq 100$ correspond to the formation of sharp lamellae boundaries. Further reorientation of lamellar under the influence of an electric field causes a gradual decline of Q_{xz} and Q_{yz} with some deviations. The xy component of the stress tensor demonstrates more interesting behavior. The intense increase of Q_{xy} is caused by growing of lamellae clusters parallel to the electric field direction, but twisted with respect to each other. Such a twist in the xy plane costs a large stress compared with other components of the stress tensor. While later disappearance of one of these clusters from $\tau \simeq 4250$ until the formation of the final structure at $\tau \simeq 17\,000$, from Fig. 6 it follows that the anisotropy factor Q_{xy} decreases. The final morphology of perfect perpendicular lamellae gives no contributions to the stress tensor due to domain deformations, consistent with the zero value reached by all anisotropy factors $Q_{\alpha\beta}$.

We also performed simulations with different surface related interaction parameters $\beta\epsilon^0_{AS}/\nu$, which led to the same final structures of perfect perpendicular lamellae shown in Fig. 7. Note that while increasing the surface related interaction parameter $\beta\epsilon^0_{AS}/\nu$ (electric field is constant), the crossover from parallel to perpendicular lamellae occurs at $\beta\epsilon^0_{AS}/\nu = 1.0$ (the adsorption energy is $0.4k_BT$) due to more dominating surface effects. Figure 7 shows an intermediate structure of two coexisting lamellae clusters of perpendicular lamellae and a final morphology in the case of interaction parameters with the surfaces $\beta\epsilon^0_{AS}/\nu = 0.5$ [Fig. 7(a)], 0.7 [Fig. 7(b)], and 0.8 [Fig. 7(c)]. In Fig. 7 one sees projections in the z direction of the external electric field. From Fig. 7 it can be concluded that a film of a block copolymer material exhibits uniaxial symmetry with respect to the applied electric field direction. The lamellae planes aligned by an electric field contain the electric field vector, but they can be oriented differently, perpendicular to the electric field plane (xy). All these states have the same energy. This type of rotational symmetry is clearly observed from the final lamellar morphologies, shown in Fig. 7, where lamellae can form in principle different angles with x and y axes. In simulations we observed only final morphologies with lamellae parallel to x or y axis (to the side box planes) due to periodic boundary conditions applied in x and y directions and due to the best

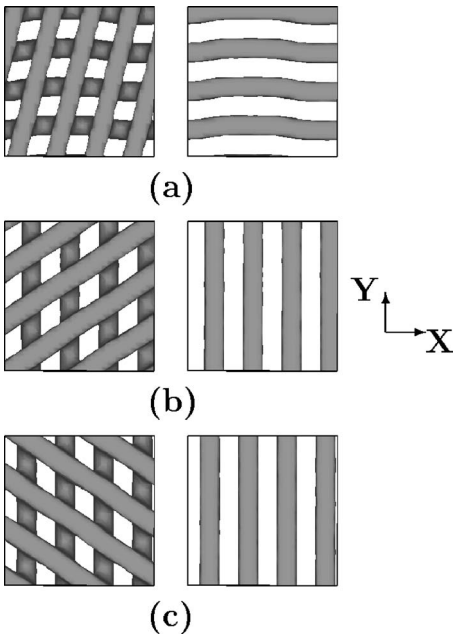

FIG. 7. An intermediate structure of two coexisting lamellae clusters of parallel to the electric field lamellae and the final morphology for the surface related interaction parameters (a) $\beta\epsilon^0_{AS}/\nu = 0.5$, (b) 0.7, and (c) 0.8. The z-axis projections in the direction of the applied electric field of the morphologies are shown.

fitting of lamellae spacing into the box size in these directions. Intermediate structures with two lamellae clusters confirm the best fitting of lamellae spacing in the case where lamellae are parallel to one of the side box planes. In these directions the integral number of lamellae matches the box size. Notice that the distance between two opposite electrode surfaces was chosen so that an integer number of lamellae fits into the film. In such a case lamellae layers are unstrained. From Fig. 7 one can see that inclined lamellae of two-cluster morphology do not fit well into the box in all slanted directions. In the slanted directions a noninteger number of lamellae fits into the box. As a result, large stresses are induced in the system (see Fig. 6). The above arguments of lamellae fitting into the box can be considered as those which model a real multigrain structure. In an actual block copolymer sample, a lamellar grain is confined within other grains and fits into some directions better than into others. Many of the grains will be oriented in directions for which the fitting is not the best, resulting in large stresses.

From Fig. 7 it follows that lamellae of two coexisting clusters can form different angles between their planes. It also confirms uniaxial symmetry inherent in a system. In general, the angle between the two clusters depends on a pathway of mesophase formation. Particularly, the distribution of defects such as holes and necks and their development in time affect the orientation of the clusters. One cluster is usually parallel to a side box plane due to above discussed reasons of lamellae fitting into the box.

The two coexisting lamellae clusters can be also treated as stable and unstable phases. In this case, the movement of a boundary between clusters is a propagation of a stable phase into an unstable phase. The inclined lamellar phase is

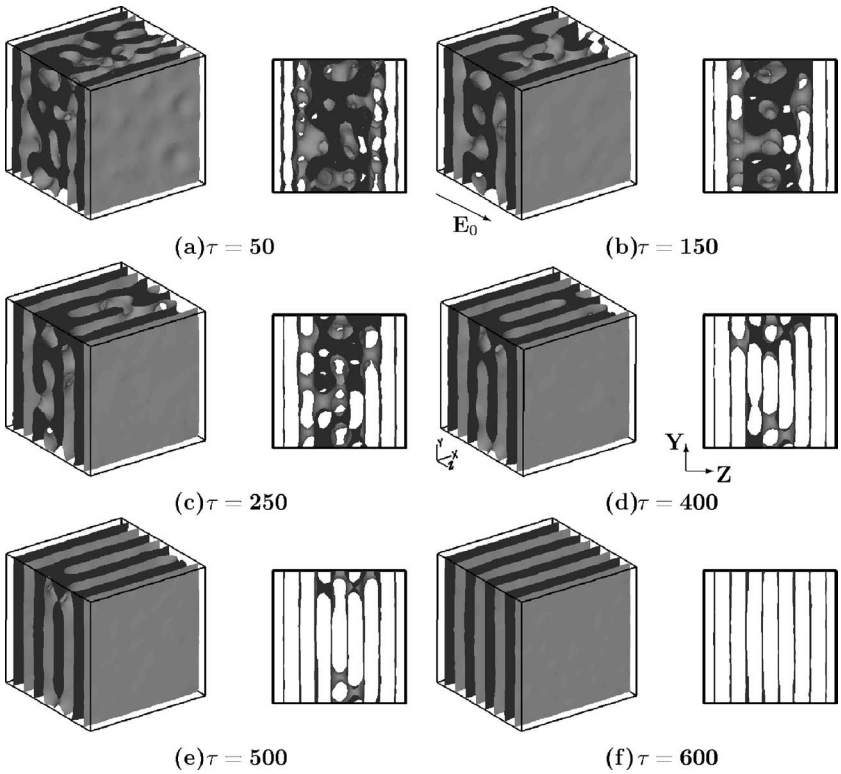

FIG. 8. Isosurface representation of an A_8B_8 diblock copolymer melt for $\nu\rho_A=0.5$ and the x projections of the lamellar morphology for the surface related interaction parameter $\beta\epsilon^0_{AS}/\nu=1.2(\beta\epsilon^0_{BS}/\nu=0.0)$, corresponding to the adsorption energy $0.48k_BT$ per statistical unit.

energetically unfavorable due to arguments of lamellae fitting into a box, and therefore it is always unstable.

Finally, we provided a simulation for the surface related interaction parameter $\beta\epsilon^0_{AS}/\nu=1.2$ (the adsorption energy is $0.48k_BT$) shown in Fig. 8. From Fig. 8 it follows that at the early stage ($\tau=50$) the forming structure is different from the growing lamellar pattern demonstrated in Fig. 1(a). The stronger interactions with surfaces lead to the nondefected adjacent to the surface lamellar layers. Instead of holes in these lamellae, observed in previous simulations with smaller surface interaction parameters, the residual undulations of adjacent layers are present, as shown in Fig. 8(a). While surfaces align lamellae, these undulations disappear and the adjacent lamellae become perfect [Fig. 8(b)]. The second pair of lamellae is already formed, but the lamellae contain many holes and connecting necks [Fig. 8(b)]. As can be concluded from Fig. 8, the mechanism of alignment is defect movement via disappearance of necks. The necks are annihilated in the direction from surfaces into bulk [Figs. 8(b)–8(e)]. After stretching and thinning, the necks break up and create curvatures in lamellae. The curvatures are not favorable for the system and are straightened during predominant surface alignment. In the end, the perfect lamellae morphology with all lamellae parallel to the surfaces is seen as a result of surface ordering [Fig. 8(f)].

The two orientational order parameters P_2 are plotted as a function of time τ in Fig. 9. The dashed curve in Fig. 9 represents the changes in lamellae orientations for the same system, but without the electric field. As can be concluded from Fig. 9, the applied electric field slows down the parallel to the surface alignment by two to three times. The reason of this is due to the fact that the necks connecting parallel lamellae are in the favorable orientation with respect to the electric field. As a result, the electric field tries to maintain the necks and to stop the neck removal. The final values of P_2 in the presence and in the absence of an electric field are the same ($P_2\simeq 0.97$) and are very close to unity, confirming a perfect parallel alignment.

The small bump in the P_2 plot is observed at $\tau\simeq 75$. This bump is also present in the case of no electric field. The nature of such behavior in lamellae orientations is a result of a process of lamellae creation. The parallel lamellae start to grow near the surfaces with further propagation inside the film. The growth of each lamellae layer from the disorder requires some time to rearrange polymer chains. During this time the global orientation of the whole sample does not

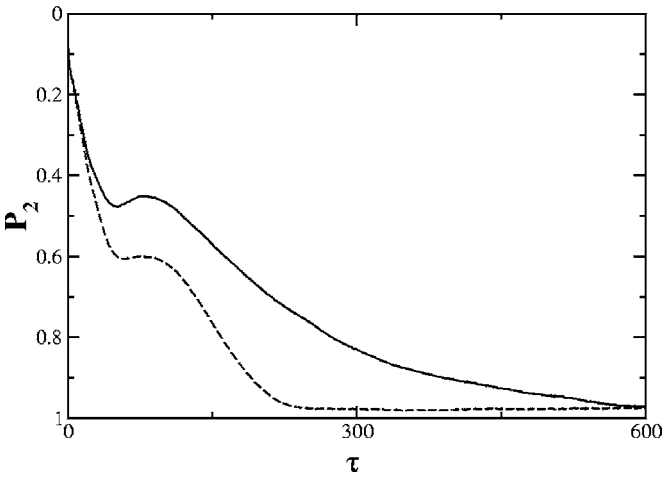

FIG. 9. Time evolution of the orientational order parameter P_2 in the presence (solid line) and in the absence (dashed line) of an external electric field. The surface related interaction parameter $\beta\epsilon^0_{AS}/\nu=1.2$ is the same for both cases.

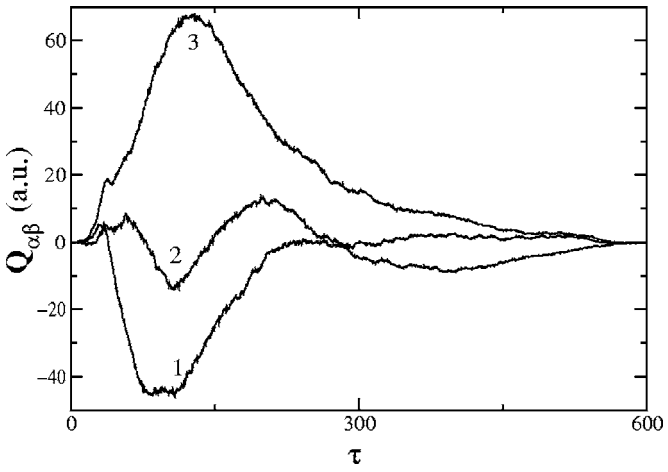

FIG. 10. Time evolution of stresses in the subjected to the electric field sample, $Q_{\alpha\beta}$, due to domain transformations: Q_{xy} (curve 1), Q_{xz} (curve 2), and Q_{yz} (curve 3). The transformations in stresses are related to morphological evolution shown in Fig. 8.

change much. Even a small decrease in P_2 is observed due to the appearance of additional necks during the new lamellae layer formation. In the presence of an electric field the decrease of P_2 is more pronounced because the orientation of the appearing necks between parallel lamellae is supported by an electric field. The growth of a pair of adjacent to the surface lamellae corresponds to the similar bump at $\tau \simeq 5$, which is hidden inside the region of the fast increasing P_2. Also, this bump is not clearly observable since its height can be compared with an amplitude of fluctuations playing the crucial role at this stage. The second bump due to formation of the second pair of lamellae layers is more pronounced. From all performed simulations we conclude that the position of the bumps does not change with varying surface related interaction parameters and is not affected by the presence of an electric field. These bumps in orientational evolution of lamellae morphology are purely an effect of ordering due to surfaces.

The anisotropy factors corresponding to the morphology evolution in Fig. 8 are plotted versus τ, as shown in Fig. 10. Only the component Q_{xz} (curve 2 in Fig. 10) exhibits large fluctuations due to creation and annihilation of differently oriented necks. The Q_{xy} (curve 1) and Q_{yz} (curve 3) increase in an absolute value with creation of sharp lamellar boundaries until $\tau \simeq 175$. Further relaxing these components to zero is affected by the surface-induced alignment via the steady removal of necks. The final structure of perfectly aligned parallel lamellae is unstressed with all stress tensor components $Q_{\alpha\beta}$ equal to zero.

Notice that the microstructure of perfectly aligned parallel lamellae shown in Fig. 8(f) is the final morphology for all simulated systems with different interactions with surfaces in the absence of an electric field.

As it follows from the performed simulations, the time scale of the electric-field-induced alignment is much higher than the time scale of the surface-induced alignment. As we observed for bulk systems,[37] the electric-field-induced alignment is very slow due to the small electrostatic contribution to the free energy of a melt. The electrostatic interactions are long-range forces and can make an effect only on ordered microdomains with rather distinct boundaries between mesophases of different dielectric properties. In contrast to electrostatic interactions, the interactions with surfaces have a short-range nature and lead to the growth of already oriented lamellae directly from a disordered state. As a result of the competition between these forces of different symmetries, the final structures can demonstrate different predominant orientations depending on the ratio of competing forces. However, at the early stage of phase separation the orientation of a microstructure is controlled by surfaces. This is confirmed by the persistent increase of the orientational order parameter P_2 in the beginning of phase separation for any realistic strength of an applied electric field.

V. CONCLUDING REMARKS

We have studied the alignment of microdomains in confined films of diblock copolymer systems exposed to an external electric field using a dynamic mean-field density functional method. In particular, the dynamic behavior of the symmetric A_8B_8 diblock copolymer melt has been investigated. The electric field induces the appearance of a perpendicular to the bounding surface lamellar microstructure. The electrode surfaces induce a parallel alignment. The total free energy of a copolymer material includes the short-range interactions of a polymer with surfaces. The surface term contributes only in the vicinity of the surfaces. The meaning of the electrostatic term included in the free energy is the long-range dipolar interaction taken as the dominant mechanism of the electric-field-induced alignment of microstructure. The driving force for the electric-field-induced alignment is the anisotropic term in the free energy of a block copolymer liquid. The mechanism of elongation and compression of chains due to the anisotropic polarizability of monomers suggested by Gurovich[20–22] is not taken into account because of its limited effect. We examined the influence of both electric fields and surfaces on the alignment kinetics in a 3D case. The results have been obtained in the intermediate segregation limit.

We have considered the block copolymer system in one initial state—a disordered (homogeneous) block copolymer melt. Starting with a disordered copolymer, the pictures of lamellar alignment in confined films in an external electric field are found to be different from the similar bulk systems.[37] The bounding surfaces presented in the system are selective for copolymer blocks and induce additional order in the sample. The simultaneously applied electric and surface fields between the block copolymer melt and electrode surfaces have different symmetries and compete with each other. Depending on the ratio between electric and surface fields, parallel or perpendicular lamellar orientations have been observed. The corresponding final structures contain no defects with no stresses due to domains.

As a consequence of the competition between the electric and surface fields, different types of alignment kinetics with different time scales have been observed. The presence of surfaces changes the kinetics of nucleation and reorientation of microdomains. There are three time scales inherent in the system: the time scale of the electric-field-induced align-

ment (relaxation time τ_E), surface alignment (τ_s), and microphase separation (τ_m). The interactions with surfaces have a short-range nature and lead to the growth of already oriented lamellae directly from the disordered state, so the time scale of the surface alignment is much smaller than the time scale of microphase separation, $\tau_s \ll \tau_m$. In contrast with surface interactions, the electrostatic interactions are long ranged and can affect only ordered microdomains with rather distinct boundaries between mesophases of different dielectric properties. Therefore, the time scale of the electric-field-induced alignment is much larger than the time scales of the surface-induced alignment and microphase separation, $\tau_E \gg \tau_m \gg \tau_s$.

APPENDIX: ELECTRIC FIELD AND ELECTROSTATIC ENERGY IN BLOCK COPOLYMER MATERIAL

To get an electric field pattern inside a dielectric copolymer material as a function of compositional order parameters $\psi_I(\mathbf{r})$ we present the complete set of Maxwell's equations describing the behavior of an electrostatic field,

$$\nabla \cdot \mathbf{D}(\mathbf{r}) = 0, \tag{A1}$$

$$\nabla \times \mathbf{E}(\mathbf{r}) = 0, \tag{A2}$$

where the electric displacement is $\mathbf{D}(\mathbf{r}) = \varepsilon(\mathbf{r})\mathbf{E}(\mathbf{r})$. Equation (A1) is solved by a method of successive approximations (perturbation method). Here, we carry out the procedure of perturbations up to the first order. The electric displacement and electric field are written as a sum of zeroth and first order terms,

$$\mathbf{D} = \mathbf{D}_{(0)} + \mathbf{D}_{(1)}, \tag{A3}$$

$$\mathbf{E} = \mathbf{E}_{(0)} + \mathbf{E}_{(1)}, \tag{A4}$$

where the zeroth order terms are related as $\mathbf{D}_{(0)}(\mathbf{r}) = \varepsilon(\mathbf{r})\mathbf{E}_{(0)}(\mathbf{r})$. The uniformly applied electric field $\mathbf{E}_0$ is considered to be a zeroth order approximation $\mathbf{E}_{(0)}$. Then, substituting Eq. (A3) into Eq. (A1), we get the perturbed equation

$$\nabla \cdot \mathbf{D}_{(1)} = -\nabla \cdot \mathbf{D}_{(0)}. \tag{A5}$$

After substituting Eq. (3) into the right part of this equation, it can be rewritten in the following form:

$$\nabla \cdot \mathbf{D}_{(1)}(\mathbf{r}) = -\nabla \cdot \left(\sum_I \varepsilon_I' \psi_I(\mathbf{r}) \mathbf{E}_0 \right). \tag{A6}$$

Equation (A2) is equivalent to the statement that an electric field is the gradient of a scalar potential $\varphi(\mathbf{r})$. The relation between the first approximation $\mathbf{D}_{(1)} = \varepsilon^0 \mathbf{E}_{(1)}$ and the scalar potential $\varphi(\mathbf{r})$ reads

$$\mathbf{D}_{(1)}(\mathbf{r}) = \varepsilon^0 \nabla \varphi(\mathbf{r}). \tag{A7}$$

Equations (A6) and (A7) yield the following equation for the potential $\varphi(\mathbf{r})$:

$$\Delta\varphi(\mathbf{r}) = -\frac{1}{\varepsilon^0} \nabla \cdot \left(\sum_I \varepsilon_I' \psi_I(\mathbf{r}) \mathbf{E}_0 \right). \tag{A8}$$

The solution of this equation, which is the Poisson equation, is well known and has the form

$$\varphi(\mathbf{r}) = \frac{1}{4\pi} \int_V \frac{1}{|\mathbf{r} - \mathbf{r}'|} \frac{1}{\varepsilon^0} \sum_I \varepsilon_I' \psi_I(\mathbf{r}) \mathbf{E}_0 d\mathbf{r}'. \tag{A9}$$

Applying the Fourier transformation of Eq. (A9) we obtain for the Fourier transform of an electric potential,

$$\varphi(\mathbf{k}) = \int_V \exp[i\mathbf{k} \cdot \mathbf{r}] \varphi(\mathbf{r}) d\mathbf{r},$$

the following expression:

$$\varphi(\mathbf{k}) = -\frac{1}{k^2} \frac{1}{\varepsilon^0} \sum_I \varepsilon_I' i k_\alpha E_{0\alpha} \psi_I(\mathbf{k}). \tag{A10}$$

Substituting the solution $\varphi(\mathbf{k})$ into the equation

$$\mathbf{E}_{(1)}(\mathbf{k}) = -i\mathbf{k}\varphi(\mathbf{k}),$$

we finally obtain the Fourier transform of the electric field in a block copolymer material to the first order of block copolymer order parameters,

$$E_\beta(\mathbf{k}) = \left[\delta_{\alpha\beta} - \sum_I \frac{\varepsilon_I'}{\varepsilon^0} \psi_I(\mathbf{k}) \hat{k}_\alpha \hat{k}_\beta \right] e_\alpha E_0, \tag{A11}$$

where $E_\beta(\mathbf{k})$ is the β component of the Fourier transform of the electric field, $\hat{k}_\alpha = k_\alpha / k$ is the α component of the unit wave vector, and e_α is the α component of the unit vector $\mathbf{e}$ of the external electric field. Equation (A11) is the generalization of Eq. (1.3) in Ref. 11.

Using Eq. (A11), the Fourier transformation of Eq. (3), and Parseval's formula, the part of the electrostatic energy in Eq. (1) which contributes to the aligning process of a block copolymer microstructure can easily be written down as Eq. (5).

Notice that the electrostatic energy (5) coincides with the induced dipolar interaction among the compositional fluctuations in nonionic fluids near the critical point.[71–73] Onuki and Doi have predicted that for near-critical fluids the dominant contribution to the Ginzburg-Landau free energy for density fluctuations due to an electric field is the dipolar interaction.[71,72]

In order to obtain the expression of electrostatic free energy in normal space we will write down the energy in the form[55,56]

$$F_{\mathrm{el}} = \frac{1}{2} \int_V \rho(\mathbf{r}) \varphi(\mathbf{r}) d\mathbf{r}, \tag{A12}$$

assuming a continuous charge density distribution $\rho(\mathbf{r})$, which satisfies the equation

$$\rho(\mathbf{r}) = -\frac{\varepsilon^0}{4\pi} \Delta\varphi(\mathbf{r}). \tag{A13}$$

With the aid of Eqs. (A8), (A9), and (A13) the free energy F_{el} is finally written in the bilinear order in the compositional order parameters as

$$F_{\mathrm{el}} = \frac{1}{32\pi^2}\frac{1}{\varepsilon^0}E_0^2\sum_{I,J}\varepsilon_I'\varepsilon_J'\int_V\int_V \frac{(\mathbf{e}\cdot\nabla\psi_I(\mathbf{r}))(\mathbf{e}\cdot\nabla\psi_J(\mathbf{r}'))}{|\mathbf{r}-\mathbf{r}'|}d\mathbf{r}d\mathbf{r}', \tag{A14}$$

where double summation covers all components, marked as I and J, of a copolymer material. The electric field E_0 in all equations can also be treated as the average electric field in a dielectric.[13] Because all relations were derived in first order approximation there is no significant difference between these two treatments of the electric field as the external electric field or as the averaged electric field in a sample.

Note that the presented approach can be employed for dielectric block copolymer materials when an external electric field is much smaller than internal molecular fields. In this case, the relation between the electric displacement and the electric field can be supposed to be linear. Thus the expressions (5) and (A14) for the free energy are well justified.

[1] F. S. Bates and G. H. Fredrickson, Phys. Today **52**(2), 32 (1999).
[2] I. W. Hamley, *The Physics of Block Copolymers* (Oxford University Press, New York, 1998).
[3] G. J. A. Sevink, A. V. Zvelindovsky, B. A. C. van Vlimmeren, N. M. Maurits, and J. G. E. M. Fraaije, J. Chem. Phys. **110**, 2250 (1999).
[4] H. P. Huinink, J. C. M. Brokken-Zijp, M. A. van Dijk, and G. J. A. Sevink, J. Chem. Phys. **112**, 2452 (2000).
[5] D. G. Walton, G. J. Kellogg, A. M. Mayes, P. Lambooy, and T. P. Russell, Macromolecules **27**, 6225 (1994).
[6] P. Sotta, S. Valić, B. Deloche, D. Maring, and H. W. Spiess, Acta Polym. **50**, 205 (1999).
[7] F. Ebert and T. Thurn-Albrecht, Macromolecules **36**, 8685 (2003).
[8] Z.-R. Chen and J. A. Kornfield, Polymer **39**, 4679 (1998).
[9] A. V. Zvelindovsky, G. J. A. Sevink, B. A. C. van Vlimmeren, N. M. Maurits, and J. G. E. M. Fraaije, Phys. Rev. E **57**, R4879 (1998).
[10] K. Amundson, E. Helfand, D. D. Davis, X. Quan, S. S. Patel, and S. D. Smith, Macromolecules **24**, 6546 (1991).
[11] K. Amundson, E. Helfand, X. Quan, and S. D. Smith, Macromolecules **26**, 2698 (1993).
[12] K. Amundson, E. Helfand, X. Quan, S. D. Hudson, and S. D. Smith, Macromolecules **27**, 6559 (1994).
[13] A. Onuki and J. Fukuda, Macromolecules **28**, 8788 (1995).
[14] J. Fukuda and A. Onuki, J. Phys. II **5**, 1107 (1995).
[15] M. W. Matsen, Phys. Rev. Lett. **95**, 258302 (2005).
[16] C.-Y. Lin, M. Schick, and D. Andelman, Macromolecules **38**, 5766 (2005).
[17] Y. Tsori, D. Andelman, C.-Y. Lin, and M. Schick, Macromolecules **39**, 289 (2006).
[18] J. Feng and E. Ruckenstein, J. Chem. Phys. **121**, 1609 (2004).
[19] M. W. Matsen, J. Chem. Phys. **124**, 074906 (2006).
[20] E. Gurovich, Macromolecules **27**, 7063 (1994).
[21] E. Gurovich, Macromolecules **27**, 7339 (1994).
[22] E. Gurovich, Phys. Rev. Lett. **74**, 482 (1995).
[23] P. Mansky, J. DeRouchey, T. P. Russell, J. Mays, M. Pitsikalis, T. Morkved, and H. Jaeger, Macromolecules **31**, 4399 (1998).
[24] T. L. Morkved, M. Lu, A. M. Urbas, E. E. Ehrichs, H. M. Jaeger, P. Mansky, and T. P. Russell, Science **273**, 931 (1996).
[25] T. L. Morkved, W. A. Lopes, J. Hahm, S. J. Sibener, and H. M. Jaeger, Polymer **39**, 3871 (1998).
[26] T. Thurn-Albrecht, J. DeRouchey, T. P. Russell, and H. M. Jaeger, Macromolecules **33**, 3250 (2000).
[27] T. Thurn-Albrecht, R. Steiner, J. DeRouchey, C. M. Stafford, E. Huang, M. Bal, M. Tuominen, C. J. Hawker, and T. P. Russell, Adv. Mater. (Weinheim, Ger.) **12**, 787 (2000).
[28] T. Thurn-Albrecht, J. DeRouchey, T. P. Russell, and R. Kolb, Macromolecules **35**, 8106 (2002).
[29] T. Xu, C. J. Hawker, and T. P. Russell, Macromolecules **36**, 6178 (2003).
[30] T. Xu, Y. Zhu, S. P. Gido, and T. P. Russell, Macromolecules **37**, 2625 (2004).
[31] J. DeRouchey, T. Thurn-Albrecht, T. P. Russell, and R. Kolb, Macromolecules **37**, 2538 (2004).
[32] T. Xu, J. T. Goldbach, and T. P. Russell, Macromolecules **36**, 7296 (2003).
[33] G. G. Pereira and D. R. M. Williams, Macromolecules **32**, 8115 (1999).
[34] B. Ashok, M. Muthukumar, and T. P. Russell, J. Chem. Phys. **115**, 1559 (2001).
[35] Y. Tsori and D. Andelman, Macromolecules **35**, 5161 (2002).
[36] Y. Tsori and D. Andelman, Interface Sci. **11**, 259 (2003).
[37] A. V. Kyrylyuk, A. V. Zvelindovsky, J. G. A. Sevink, and J. G. E. M. Fraaije, Macromolecules **35**, 1473 (2002).
[38] A. V. Kyrylyuk, J. G. A. Sevink, A. V. Zvelindovsky, and J. G. E. M. Fraaije, Macromol. Theory Simul. **12**, 508 (2003).
[39] N. Yamazaki, M. Motoyama, M. Nonomura, and T. Ohta, J. Chem. Phys. **120**, 3949 (2004).
[40] A. V. Kyrylyuk and J. G. E. M. Fraaije, Macromolecules **38**, 8546 (2005).
[41] R. Weidisch, M. Stamm, G. H. Michler, H. Fischer, and R. Jerome, Macromolecules **32**, 742 (1999).
[42] T. Taniguchi, K. Sato, and M. Doi, in *Statistical Physics*, edited by M. Tokuyama and H. E. Stanley (AIP, Melville, NY, 2000), Paper No. CP519, p. 581.
[43] G. Venugopal and S. Krause, Macromolecules **25**, 4626 (1992).
[44] G. Venugopal, S. Krause, and G. E. Wnek, Polymer **34**, 3241 (1993); Chem. Mater. **4**, 1334 (1992).
[45] K. Xi and S. Krause, Macromolecules **31**, 3974 (1998).
[46] D. Wirtz, K. Berend, and G. G. Fuller, Macromolecules **25**, 7234 (1992).
[47] D. Wirtz, D. E. Werner, and G. G. Fuller, J. Chem. Phys. **101**, 1679 (1994).
[48] D. Wirtz and G. G. Fuller, Phys. Rev. Lett. **71**, 2236 (1993).
[49] E. Gurovich, Macromolecules **28**, 6078 (1995).
[50] A. Böker, A. Knoll, H. Elbs, V. Abetz, A. H. E. Müller, and G. Krausch, Macromolecules **35**, 1319 (2002).
[51] A. Böker, H. Elbs, H. Hänsel, A. Knoll, S. Ludwigs, H. Zettl, V. Urban, V. Abetz, A. H. E. Müller, and G. Krausch, Phys. Rev. Lett. **89**, 135502 (2002).
[52] A. Böker, K. Schmidt, A. Knoll, H. Zettl, H. Hänsel, V. Urban, V. Abetz, and G. Krausch, Polymer **47**, 849 (2006).
[53] T. Thurn-Albrecht, J. Schotter, G. A. Kästle, N. Emley, T. Shibauchi, L. Krusin-Elbaum, K. Guarini, C. T. Black, M. T. Tuominen, and T. P. Russell, Science **290**, 2126 (2000).
[54] M. Park, C. Harrison, P. M. Chaikin, R. A. Register, and D. Adamson, Science **276**, 1401 (1997).
[55] L. D. Landau and E. M. Lifshitz, *Electrodynamics of Continuos Media* (Pergamon, New York, 1984).
[56] J. D. Jackson, *Classical Electrodynamics* (Wiley, New York, 1975).
[57] L. D. Landau, E. M. Lifshitz, and L. P. Pitaevskii, *Statistical Physics* (Pergamon, New York, 1980).
[58] L. Leibler, Macromolecules **13**, 1602 (1980).
[59] J. G. E. M. Fraaije, B. A. C. van Vlimmeren, N. M. Maurits, M. Postma, O. A. Evers, C. Hoffmann, P. Altevogt, and G. Goldbeck-Wood, J. Chem. Phys. **106**, 4260 (1997).
[60] G. J. A. Sevink, J. G. E. M. Fraaije, and H. P. Huinink, Macromolecules **35**, 1848 (2002).
[61] G. J. A. Sevink, A. V. Zvelindovsky, J. G. E. M. Fraaije, and H. P. Huinink, J. Chem. Phys. **115**, 8226 (2001).
[62] P. C. Hohenberg and B. I. Halperin, Rev. Mod. Phys. **49**, 435 (1977).
[63] N. M. Maurits and J. G. E. M. Fraaije, J. Chem. Phys. **107**, 5879 (1997).
[64] N. M. Maurits, B. A. C. van Vlimmeren, and J. G. E. M. Fraaije, Phys. Rev. E **56**, 816 (1997).
[65] A. Onuki, Phys. Rev. A **35**, 5149 (1987).
[66] A. Onuki, J. Phys.: Condens. Matter **9**, 6119 (1997).
[67] T. Ohta, H. Nozaki, and M. Doi, Phys. Lett. A **145**, 304 (1990).
[68] H. F. Scherk, J. Reine Angew. Math. **13**, 185 (1835).
[69] S. P. Gido, J. Gunther, E. L. Thomas, and D. Hoffman, Macromolecules **26**, 4506 (1993).
[70] S. P. Gido and E. L. Thomas, Macromolecules **27**, 849 (1994).
[71] A. Onuki and M. Doi, Europhys. Lett. **17**, 63 (1992).
[72] A. Onuki, Europhys. Lett. **29**, 611 (1995).
[73] A. Onuki, Physica A **217**, 38 (1995).